Archived at the Flinders Academic Commons:
http://dspace.flinders.edu.au/dspace/

The following article appeared as: Palihawadana, P., Sullivan, J.P., Buckman, S.J., Masin, Z., Gorfinkiel, J.D., Blanco, F., Garcia, G. and Brunger, M.J., 2013. A joint theoretical and experimental study for elastic electron scattering from 1,4-dioxane. Journal of Chemical Physics, 139, 014308.

and may be found at:

http://jcp.aip.org/resource/1/jcpsa6/v139/i1/p014308_s1

DOI: http://dx.doi.org/10.1063/1.4807610

A joint theoretical and experimental study for elastic electron scattering from 1,4-dioxane

P. Palihawadana,[1] J. P. Sullivan,[1] S. J. Buckman,[1,2] Z. Mašín,[3] J. D. Gorfinkiel,[3] F. Blanco,[4] G. García,[5,6] and M. J. Brunger[2,7,a)]

[1]*Centre for Antimatter-Matter Studies, Research School of Physics and Engineering, Australian National University, Canberra ACT 0200, Australia*

[2]*Institute of Mathematical Sciences, University of Malaya, Kuala Lumpur 50603, Malaysia*

[3]*Department of Physical Sciences, The Open University, Walton Hall, Milton Keynes MK7 6AA, United Kingdom*

[4]*Departmento de Física Atómica, Molecular y Nuclear, Universidad Complutense de Madrid, Madrid E-28040, Spain*

[5]*Instituto de Física Fundamental, Consejo Superior de Investigaciones Científicas, Madrid E-28006, Spain*

[6]*Centre for Medical Radiation Physics, University of Wollongong, Wollongong, NSW 2522, Australia*

[7]*Centre for Antimatter-Matter Studies, School of Chemical and Physical Sciences, Flinders University, GPO Box 2100, Adelaide SA 5001, Australia*

We present results of measurements and calculations of elastic electron scattering from 1,4-dioxane in the energy range of 0–1000 eV. Absolute differential and integral elastic cross sections have been measured using a crossed electron-molecule beam spectrometer and the relative flow technique, at four energies in the 10–30 eV range and for scattered electrons in the angular range $20°$–$129°$. The measured cross sections are compared with results from R-matrix computations, at the static exchange plus polarization level, calculated at energies between 0–20 eV, and with calculations employing the independent atom model with the screening corrected additivity rule (IAM-SCAR). Those latter computations were conducted at energies between 1 and 1000 eV. Agreement between the measured and R-matrix cross sections was typically found to be good at all common energies, whereas agreement with IAM-SCAR was satisfactory only at 30 eV. To the best of our knowledge, the present results are the first absolute data to be published in the literature for this scattering system. © *2013 AIP Publishing LLC*. [http://dx.doi.org/10.1063/1.4812215]

I. INTRODUCTION

Within the scientific community, particular interest has developed over the last 13 or so years to investigate the effect that low energy charged particles may cause within the human body,[1] specifically during medical therapies or diagnostic tests. While most medical devices initially begin with very high-energy photons (e.g., X-rays), electrons, or positrons (e.g., in positron emission tomography), this high-energy radiation quickly thermalises in the body through processes such as direct ionization which in turn leads to the liberation of a significant number of lower energy secondary electrons. Those secondary electrons may subsequently attach to the various components of DNA, causing important cell and tissue damage.[2,3] These are just some of the reasons why it is interesting to study the interaction between low energy electrons and those molecules which can be considered as the "building blocks" of DNA.

As a consequence of the above, there are now several groups (see, e.g., Refs. 4–9 and references therein) using Monte Carlo simulation techniques in order to study particle tracks as those particles traverse through matter. Such studies ultimately aim to provide a nano-scale description of radiation damage in matter, and most if not all require a significant database for the relevant atomic and molecular (ATMOP) processes that are occurring.[6] Such an extensive database should also be as accurate and reliable as possible. Two components of such an ATMOP database are the elastic differential and integral cross sections. We have therefore been undertaking a systematic study on measuring cross sections for electron scattering from a class of organic molecules, known generally as cyclic ethers, that might be considered as moieties to nucleotides in living matter. Previous work includes scattering from tetrahydrofuran[10–13] and 3-hydroxy-tetrahydrofuran,[14] while in the present investigation we report new measured differential cross sections (DCSs) and integral cross sections (ICSs) for elastic electron scattering from 1,4-dioxane ($C_4H_8O_2$) – see Fig. 1. To assist us in better understanding our measured results for $C_4H_8O_2$, we have also undertaken R-matrix calculations[15,16] at the static exchange plus polarization level and independent atom model with screening corrected additivity rule (IAM-SCAR) computations.[17] To the best of our knowledge there are currently no other absolute experimental or theoretical results for electron scattering from 1,4-dioxane, with only a single study, known to us,[18] using positrons as the probe. Note, however, that some relative electron energy loss spectra were determined[19] in the early 1990s and are available.

1,4-dioxane and pyrazine can both be thought of as being benzene (C_6H_6) derivatives (see Fig. 1). In addition, all
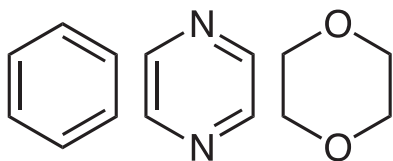
FIG. 1. Schematic diagram showing the structures of benzene, pyrazine, and 1,4-dioxane (as going from left to right).

three molecules, to one degree or another, exhibit quite similar physico-chemical properties. For instance, benzene has an isotropic dipole polarizability (α) of $\sim$68.9 a.u.,[20] with the corresponding value for pyrazine being $\sim$60 a.u.[21] and that for 1,4-dioxane being $\sim$58.79 a.u.[22] Similarly, as a consequence of their very high symmetry (see. Fig. 1), all three molecules have no permanent dipole moment (i.e., $\mu \sim 0$ D). It is thus interesting, and possibly quite instructive, to compare the scattering cross sections for these three molecules to see if any trends emerge and whether or not those trends can be associated with their intrinsic physico-chemical properties. Such a comparison is only now possible due to recent detailed studies on pyrazine,[23,24] earlier work on benzene[25,26] and the current measurements with 1,4-dioxane. Note that this systematic comparison of the scattering behaviour for benzene, pyrazine, and 1,4-dioxane (see Fig. 1) also forms a rationale behind the present work.

Details of the experimental apparatus and techniques are explained in Sec. II, with an exposition on our theoretical approaches being given in Sec. III. The present results and a discussion of those results, including a detailed comparison between our measured and calculated cross sections, follows in Sec. IV. Finally, in Sec. V, some concluding remarks are made.

II. EXPERIMENTAL APPARATUS AND TECHNIQUES

A crossed electron-molecular beam apparatus was used to measure the elastic electron scattering cross sections from 1,4-dioxane. A detailed description of this spectrometer has been given previously (e.g., Ref. 27), so that only a précis is given below. Note, however, that since the description in Gibson *et al.*[27] a fully computer-controlled hardware and controlling LabVIEW software to support it have been implemented. That development assisted with both the optimisation of the incident electron beam current and its energy resolution. In addition, the data acquisition, analysis, and real-time monitoring of all the experimental parameters is handled by the new computer system.

The energy of the incident electron beam is calibrated against the position of the known $1s\,2s^2\,{}^2S$ negative-ion resonance in the helium (He) elastic channel, at 19.365 eV.[28] The overall energy resolution of the spectrometer is about 70 meV (FWHM) for the present results, which means that our elastic measurements are in fact rotationally averaged. Furthermore, as the lowest vibrational modes of 1,4-dioxane can be excited at $\sim$40 meV some vibrational averaging also occurs. Depending on the specific energy of the electron beam, the incident beam current, as measured with a Faraday Cup, varied between 1–2 nA. The electron beam profile and

current were optimised under computer control in order to obtain the best possible signal to background ratio for the scattering experiments. The electron analyser is capable of measuring DCSs over an angular range of $\sim -20°$–130° about the incident electron beam direction. The angular resolution of the present measurements is typically $\pm 1°$. The true zero degree position of the analyser is determined by extrapolating to the maximum of the scattered electron signal from the measurements on either side of the mechanical zero position. We estimate this to be accurate to about $\pm 0.5°$.

A high purity (99.8%) anhydrous 1,4-dioxane liquid sample/bottle, purchased from Sigma-Aldrich, is used to generate the 1,4-dioxane vapour. At room temperature this produced a vapour pressure of $\sim$30 Torr, which was sufficient to provide a stable source for the target molecular beam. The molecular beam is formed by quasi-effusive flow of the gas through a capillary needle, 15 mm long and 0.75 mm in diameter. In this investigation the temperature of the gas lines and valves that controlled the flow of the gas was kept at around 28 °C (i.e., 5 °C above the controlled room temperature of 23 °C), in order to help prevent any condensation of the 1,4-dioxane on the inner walls of the gas lines and valves. Both the pressure and temperature were monitored and controlled by the new computer-controlled hardware system. The temperature variations during our measurements were within ± 1 °C, while the change in the 1,4-dioxane pressure was less than 3%.

The relative flow technique[29] is employed to obtain absolute elastic cross sections by comparing the scattered electron signals from 1,4-dioxane with those from helium. Helium is used as the reference gas as its elastic DCSs are well established and have been considered as a "benchmark" for many years in the field. For energies below 20 eV, the He cross sections of Nesbet[30] are used, whereas for higher energies the rational function fits of Boesten and Tanaka[31] to a range of previous measurements (e.g., Ref. 32) of the He cross sections are used. The elastic DCS of 1,4-dioxane (Diox), at a given incident electron energy (E_0) and scattered electron angle (θ), is derived using the formula

$$\mathrm{DCS}_{\mathrm{Diox}}(E_0, \theta) = \frac{(N_{\mathrm{Diox}} - N_B)}{(N_{\mathrm{He}} - N_B)}$$
$$\cdot \frac{F_{\mathrm{He}} \cdot \sqrt{M_{\mathrm{He}}}}{F_{\mathrm{Diox}} \cdot \sqrt{M_{\mathrm{Diox}}}} \cdot \mathrm{DCS}_{\mathrm{He}}(E_0, \theta), \quad (1)$$

where $\mathrm{DCS}_{\mathrm{Diox}}(E_0, \theta)$ and $\mathrm{DCS}_{\mathrm{He}}(E_0, \theta)$ are the absolute DCSs for elastic scattering from 1,4-dioxane and He, N_{Diox} and N_{He} are the measured scattering signals from the 1,4-dioxane and helium gases [with the background scattering (N_B) contribution subtracted from both measurements], F_{Diox} and F_{He} are the measured relative flow rates and M_{Diox} and M_{He} are the molecular weights of 1,4-dioxane and helium, respectively. Note that all the scattering signals (N_{Diox}, N_{He}, and N_B) mentioned above are corrected for any variation in the electron beam current during the measurement cycle. ICS(E_0) are subsequently derived from our measured DCS, in a manner described later in Sec. IV.

The ratio of the driving pressures between 1,4-dioxane and helium is selected to satisfy the condition that their collisional mean free paths are the same in the beam-forming

capillary. This is done to try and ensure that the collision-dependent spatial profiles of the gas beams are largely identical in the interaction region. In this work, this implied a helium to 1,4-dioxane ratio of $\sim$6, with the typical driving pressures for each species being in the range 0.9–1.0 Torr for helium and 0.15–0.17 Torr for 1,4-dioxane. Note that during the course of our measurements we allowed on occasion the helium to 1,4-dioxane ratio to vary by up to 10% from the optimum value, with no noticeable effect, to within our measurement uncertainties, being found on the derived 1,4-dioxane absolute DCSs. The overall uncertainty, both statistical and systematic, of this work is between $\sim$7.3% and 16%, but for the overwhelming majority of determinations it lies below 8.5%.

III. THEORY DETAILS

A. R-matrix calculations

The R-matrix method[15] and its application to electron-molecule scattering[33] have been recently described in detail. We will nonetheless briefly summarize the method here. The key idea of the R-matrix method is the division of configuration space into two regions, an inner and an outer region. These are separated by a sphere of radius $r = a$ centred on the centre of mass of the system. The R-matrix sphere must be large enough to contain the charge density of the target states of interest and that associated with the target orbitals used to build the L^2 functions (see below). The more complex inner region problem is solved first. In this region, the wavefunction for the N + 1 electron system can be written as follows:

$$\Psi_k^\Gamma(\mathbf{X_1}\ldots\mathbf{X_{N+1}}) = \mathcal{A}\sum_{i=1}^{n}\sum_{j=1}^{n_c}\Phi_i(\mathbf{X_1}\ldots\mathbf{X_N};\hat{r}_{N+1};\sigma_{N+1})$$
$$\times\frac{u_{ij}(r_{N+1})}{r_{N+1}}a_{ijk}$$
$$+\sum_{i=1}^{m}\chi_i(\mathbf{X_1}\ldots\mathbf{X_{N+1}})b_{ik}, \qquad (2)$$

where $\mathbf{X_i}$ represent the space and spin coordinates of electron i and $\sigma_{\mathbf{N+1}}$ indicates the spin coordinates of the (N + 1)th electron. The operator $\mathcal{A}$ ensures the antisymmetrization of the whole wavefunction. The functions $\Phi_i(\mathbf{X_N};\hat{r}_{N+1};\sigma_{N+1})$ are built as products of the target wavefunctions $\Phi_i(\mathbf{X_N})$ of each of the n states included in the calculation and the angular (spherical harmonics) and spin functions of the scattering electron. The functions u_{ij} describe the radial behaviour of the scattering electron and are generated as linear combinations of Gaussian functions centred on the centre of mass of the molecule. The L^2-integrable functions $\chi_i(\mathbf{X_{N+1}})$, built as products of target orbitals, are crucial for the representation of short-range correlation and polarization effects. The spin-space symmetry of the wavefunctions is denoted by Γ. In order to obtain the coefficients a_{ijk} and b_{ik}, we diagonalize the matrix obtained from the sum of the N + 1 Hamiltonian and the Bloch operator.[15] This generates a set of wavefunctions Ψ_k^Γ and their associated eigenvalues, E_k.

In the outer region, where exchange between the scattering and target electrons can be neglected, a single centre expansion of the electron-molecule interaction is used. The radial functions describing the behaviour of the scattering electron are determined by solving a set of coupled differential equations. This is done by propagating the R-matrix, constructed using inner region (Ψ_k^Γ and E_k) and target electronic (energies and transition moments) information. The propagation is carried out to a radius large enough so that an asymptotic expansion for the radial wavefunctions of the scattering electron in each channel can be used. K-matrices are determined by matching these to known analytical asymptotic solutions. Integral and differential cross sections, resonances' properties, etc., can be obtained from them.

The R-matrix calculations reported in this work have been performed within the fixed-nuclei approximation using the UKRmol suite.[34] POLYDCS[35] was used to determine the DCS.

1,4-Dioxane, $C_4H_8O_2$, has a vertical ionization energy[36] of around 9.4 eV and its spherical polarizability[37] is in the range 40–60 a_0^3. It belongs to the C_{2h} point group and is therefore a non-polar molecule. The calculations presented here are based on the experience gained in the study of electron collisions with the diazines[16,23] ($C_4H_4N_2$), especially with pyrazine.

We employed a geometry of the molecule optimised[37] using density functional theory (B3LYP and 6-311+G(3df,2p) basis set). Following our earlier work, we performed calculations with two different basis sets: a compact, 6-311G(d,p), and one containing diffuse functions, 6-311+G(d,p) at the SE and SEP (static-exchange and static-exchange plus polarization) levels. Since we are only interested in elastic cross sections, we did not perform calculations that involved electronically excited states (that is, we did not perform calculations at the close-coupling level; or, in other words, only the wavefunction for the target ground state was included in Eq. (2)). In addition, work on the diazines has led us to conclude that the SEP model allows us to better represent short range polarization and correlation effects: changing the number of orbitals included in the virtual space allows us to tune these effects.[23] This model is better at providing accurate positions for low-lying shape resonances and describing a Ramsauer-Townsend minimum if these are present.

In the SE and SEP models, the target ground state is described at the Hartree-Fock (HF) level. We generated HF-SCF orbitals that are used both for the target wavefunction and to build the L^2 functions. The ground state energies obtained for dioxane are -305.902 H and -305.909 H for the compact and diffuse basis set, respectively. The polarization of the molecule is described in the SEP model by configurations in which one electron from the occupied orbitals is promoted to the selected virtual orbitals (unoccupied in the Hartree-Fock ground state configuration), which are also available for the scattering electron.

In order to ensure that the electronic density of both the target ground state and the L^2 functions is contained inside the R-matrix sphere, a radius $a = 13a_0$ when using the compact basis set and $a = 18a_0$ when using the diffuse basis set were required. The appropriate continuum GTOs

basis sets,[38,39] including partial waves up to $l = 4$, were employed.

Following our work on diazines, we investigated the dependence of the cross sections on the number of virtual orbitals used. The results using the diffuse basis set displayed what looked like non-physical structures that were very dependent on the number of virtual orbitals. We therefore deemed these results unreliable and, in Secs. III A and IV, report only results corresponding to the use of the compact basis set and 25 or 40 virtual orbitals.

We employed the time-delay method for the analysis and characterization of the resonances present in the system. The use of this method in the context of our calculations has been described before.[40] Briefly, for each scattering energy we use the **K**-matrix to generate the **S**-matrix which is then used to calculate the time-delay matrix **Q**. The time-delay matrix is diagonalized and its eigenvalues as a function of the scattering energy are plotted and analyzed. Resonances appearing in the system are then revealed as Lorentzian peaks in the plots of the **Q**-matrix eigenvalues.

POLYDCS uses a frame transformation to generate the DCS. This reintroduces their dependence on the initial and final rotational states of the target molecule. Our elastic differential cross sections are therefore calculated summing over final rotational states (and assuming the molecule is initially in the ground rotational state). We have found that for 1,4-dioxane (as is also the case for the diazines) this sum needs to be extended to states with $j = 9$ in order to ensure the cross sections have converged. This is not the case for targets like water or methane where summing to $j = 5$ or 6 is sufficient.

B. Independent atom model calculations

Cross sections for elastic electron scattering from 1,4-dioxane were also calculated using a screening-corrected form of the IAM model.[41–43] The first subjects of the present calculations are the atoms constituting 1,4-dioxane, namely, C, O, and H. We represent each atomic target by an interacting complex potential (i.e., the optical potential), whose real part accounts for the elastic scattering of the incident electrons, while the imaginary part represents the inelastic processes that are considered as "absorption" from the incident beam. To construct this complex potential for each atom, the real part is represented by the sum of three terms: (i) a static term derived from a Hartree-Fock calculation of the atomic charge distribution,[44] (ii) an exchange term to account for the indistinguishability of the incident and target electrons,[45] and (iii) a polarization term[46] for the long-range interactions which depend on the target dipole polarizability. The imaginary part, following the procedure of Staszewska *et al.*,[47] then treats inelastic scattering as electron-electron collisions. However, we initially found some major discrepancies in the available scattering data, which were subsequently corrected when a more physical formulation of the absorption potential[48] was introduced. Further improvements to the original formulation,[47] such as the inclusion of screening effects, local velocity corrections, and in the description of the electrons' indistinguishability,[41] finally led to a model that pro-

vides a good approximation of electron-atom scattering over a broad energy range. An excellent example of this was for elastic electron atomic iodine scattering,[49] where the optical potential results compared very favourably with those from an independent, highly sophisticated, Dirac B-spline R-matrix computation.

To calculate the cross sections for electron scattering from 1,4-dioxane, we follow the IAM by applying what is commonly known as the additivity rule (AR). In this approach, the molecular scattering amplitude is derived from the sum of all the relevant atomic amplitudes, including the phase coefficients, which lead to the molecular DCSs for the species in question. Integral cross sections can then be determined by integrating those DCSs, with the sum of the elastic ICS and the absorption ICS (for all inelastic processes except rotations and vibrations) then giving the total cross sections. Alternatively, the ICSs for 1,4-dioxane can also be derived from the relevant atomic ICSs in conjunction with the optical theorem.[41] Unfortunately, in its original form, we found an inherent contradiction between the ICSs derived from those two approaches, which suggested the optical theorem was being violated.[50] This conundrum, however, has been resolved[51] by employing a normalisation during the computation of the DCSs, so that the ICSs derived from the two approaches are now entirely consistent.[50] Nonetheless this normalisation approach does come at a cost, as is well illustrated in Fig. 2. Here we see that an apparent discontinuity is introduced into the respective IAM-SCAR elastic angular distributions at some (energy-dependent) scattering angle. We believe, however, that this is a small price to pay to ensure self-consistency between the results from the two approaches in calculating the ICSs.

A limitation of the AR is that no molecular structure is considered, so that it is really only applicable when the incident electrons are so fast that they effectively see the target molecule as a sum of individual atoms (typically
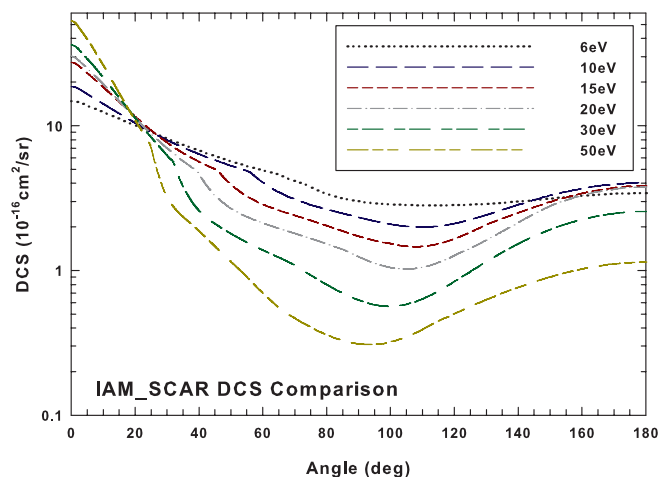

FIG. 2. A selection of the present IAM-SCAR elastic DCS for electron scattering from 1,4-dioxane. See also the legend in the figure. Note the change of slope at a particular angle at each energy, in the angular distributions, due to the normalisation procedure introduced in the IAM-SCAR method (see text for details). Please note that tables of the IAM-SCAR elastic DCS, for energies between 1 and 1000 eV, are available on request from the corresponding author.

above $\sim$100 eV). To reduce this limitation García and co-workers[43,51] introduced the SCAR method, which considers the geometry of the relevant molecule (atomic positions and bond lengths) by using some screening coefficients (SC). With this correction, the range of validity of the IAM-SCAR approach might be extended to incident energies of 30 eV or a little lower (see e.g., Refs. 17, 52, and 53).

IV. RESULTS AND DISCUSSION

Our measured absolute DCSs for elastic scattering of electrons from 1,4-dioxane are listed in Table I, along with their associated absolute errors. Also included in Table I at the foot of each column are the absolute ICSs (and error) for each incident energy, while in Table II a selection of our IAM-SCAR elastic ICSs are presented for energies between 1 and 1000 eV. In Figs. 3–6, we compare the present DCS measurements at 10, 15, 20, and 30 eV, respectively, with our IAM-SCAR and R-matrix results. There are no previous DCS 1,4-dioxane measurements that we are aware of, however, corresponding results for scattering from benzene[25,26] and pyrazine[24] are included throughout Figs. 3–6. Our measured ICSs are shown in Fig. 7, where they are compared against the results of our calculations. Note that in all cases, the R-matrix data are those calculated to within the SEP level of approximation and for the cases of 25 virtual orbitals and 40 virtual orbitals. Assuming the inelastic cross section is about 10% of the elastic one (as is the case for pyrazine[23]) we do not expect the integral elastic cross section to change by more than this percentage when inelastic channels are included in the calculation. Similarly, this inclusion is unlikely to change the shape of the R-matrix DCS significantly.

Considering now Fig. 3 for an impact energy of 10 eV in detail, we observe very good quantitative agreement between our measurements and the R-matrix-SEP calculation with 40 virtual orbitals included. The comparison with the calcula-

TABLE I. Absolute experimental DCSs for elastic scattering from 1,4-dioxane in units of 10^{-16} cm^2 sr^{-1}. The absolute uncertainty is given in parentheses. The ICS for each incident energy is given in units of 10^{-16} cm^2 at the base of each column. The absolute uncertainty on the ICS is also given in parentheses.

Scattering angle (deg)	Incident energy (eV)			
	10 eV DCS	15 eV DCS	20 eV DCS	30 eV DCS
20	13.5(2.0)	17.1(1.6)	15.4(1.7)	19.1(2.2)
30	7.30(0.59)	5.21(0.41)	3.16(0.24)	3.18(0.28)
40	2.72(0.20)	1.79(0.13)	1.51(0.11)	1.80(0.15)
50	1.60(0.12)	1.45(0.11)	1.45(0.11)	1.60(0.13)
60	1.34(0.10)	1.25(0.10)	1.44(0.11)	1.11(0.10)
70	1.37(0.11)	1.14(0.09)	1.22(0.09)	0.751(0.060)
80	1.68(0.15)	1.05(0.08)	0.977(0.074)	0.518(0.041)
90	1.70(0.13)	1.09(0.12)	0.835(0.075)	0.462(0.041)
100	1.76(0.14)	1.10(0.09)	0.915(0.070)	0.532(0.045)
110	1.64(0.12)	1.31(0.10)	0.960(0.070)	0.710(0.063)
120	1.76(0.13)	1.35(0.10)	1.11(0.08)	1.01(0.10)
129	2.09(0.16)	1.48(0.12)	1.34(0.10)	1.25(0.12)
ICS	37.0(9.3)	32.2(8.1)	28.4(7.1)	27.3(6.8)

TABLE II. Present IAM-SCAR elastic ICS (10^{-16} cm^2) for electron scattering from 1,4-dioxane.

Energy (eV)	Elastic ICS (10^{-16} cm^2)
1	82.6
1.5	76.4
2	70.6
3	61.3
4	58.0
5	55.2
7	51.0
10	47.0
15	40.9
20	34.4
30	26.1
40	22.0
50	19.4
70	16.0
100	13.2
150	10.6
200	8.99
300	7.08
400	5.91
500	5.12
700	4.06
1000	3.14

tion including 25 virtual orbitals is somewhat poorer. The two minima seen in both the experimental and theoretical angular distributions, which are in good accord with one another, appear at somewhat smaller scattering angles than those observed in the case of pyrazine.[23,24] The level of agreement at 10 eV between the present measured and IAM-SCAR calculated DCS is, however, rather poor. This comes as no surprise, as the screening corrections to the additivity rule, to account for the molecular structure of 1,4-dioxane, are not expected to
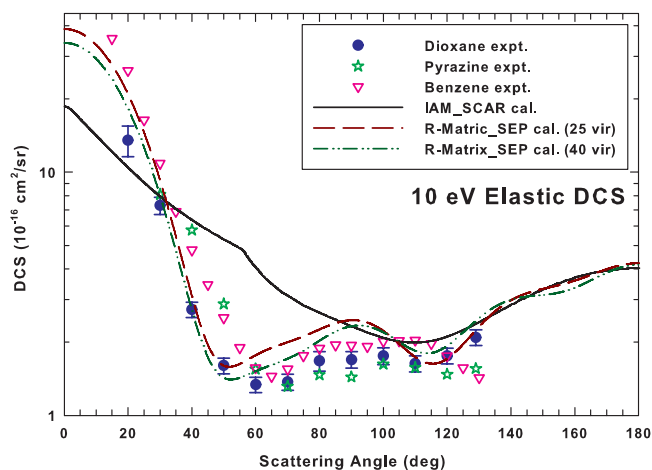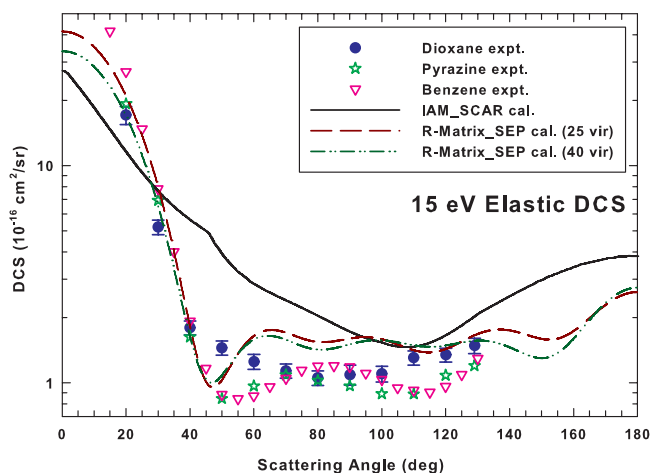

FIG. 3. Absolute DCS for elastic electron scattering from 1,4-dioxane at 10 eV. The present 1,4-dioxane measurements ($\bullet$) are compared against earlier benzene ($\triangledown$)[25,26] and pyrazine ($\star$)[24] results and to our current IAM-SCAR (———) and R-matrix (— — —) 25 virtual orbitals and R-matrix (— $\cdot \cdot$ —) 40 virtual orbital computations.

FIG. 4. Absolute DCS for elastic electron scattering from 1,4-dioxane at 15 eV. The present 1,4-dioxane measurements (●) are compared against earlier benzene (▽)[25,26] and pyrazine (☆)[24] results and to our current IAM-SCAR (———) and R-matrix (— — —) 25 virtual orbitals and R-matrix (— · · —) 40 virtual orbital computations.

FIG. 6. Absolute DCS for elastic electron scattering from 1,4-dioxane at 30 eV. The present 1,4-dioxane measurements (●) are compared against earlier benzene (▽)[25,26] and pyrazine (☆)[24] results and to our current IAM-SCAR (———) computations.

be accurate at such a low energy. This is indeed reflected in what we observe in Fig. 3.

A similar situation to that at 10 eV is also seen in Fig. 4 for our 15 eV elastic 1,4-dioxane DCS. In this case the agreement between our R-matrix-SEP with 40 virtual orbitals calculation and the measured data are relatively poorer at 15 eV compared to that at 10 eV, although overall we would still characterize their level of accord as being rather good. There is little difference (in particular with regards to the experimental errors) between the calculations using 25 and 40 virtual orbitals in this case. We believe that the relatively poorer agreement at 15 eV is very likely to be due to the limitations of the calculations, among others, due to the non-inclusion of electronic-state excitation or ionization channels. It should also be noted that above about 13 eV (see Fig. 7) non-physical pseudoresonances are present in the R-matrix results. This is a standard feature of SEP results[15] when using a multicon-
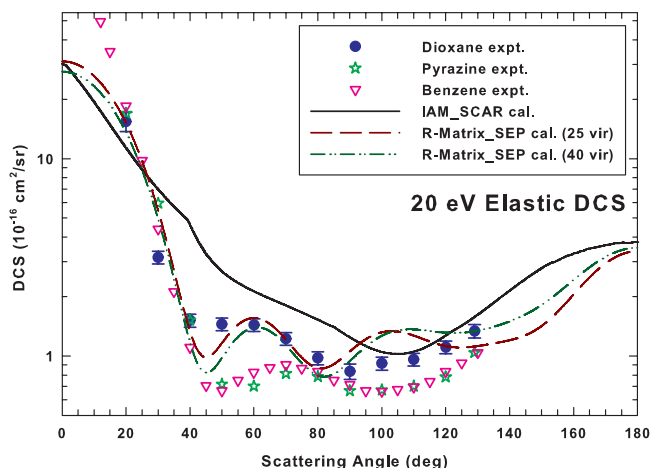
figuration description for the (N+1) electron wavefunction. Finally, we note that the agreement between the IAM-SCAR calculation and measured data at 15 eV remains poor (see Fig. 4).

Given the limitations of the R-matrix-SEP calculations at higher energies, the level of agreement between our 20 eV R-matrix results and the measured DCS is really quite remarkable (see Fig. 5) and remains quite good. We believe this statement holds even though there is clearly more pronounced structure in the R-matrix angular distribution than in the measured angular distribution, in an extension of what is observed at 15 eV. While the level of agreement between our measured 20 eV DCS and the corresponding IAM-SCAR calculation is improved, compared to what we saw earlier at 10 eV and 15 eV, in absolute terms it remains unsatisfactory. We reiterate that this observation simply reflects the expected breakdown in our screening corrections approach at these lower incident electron energies.
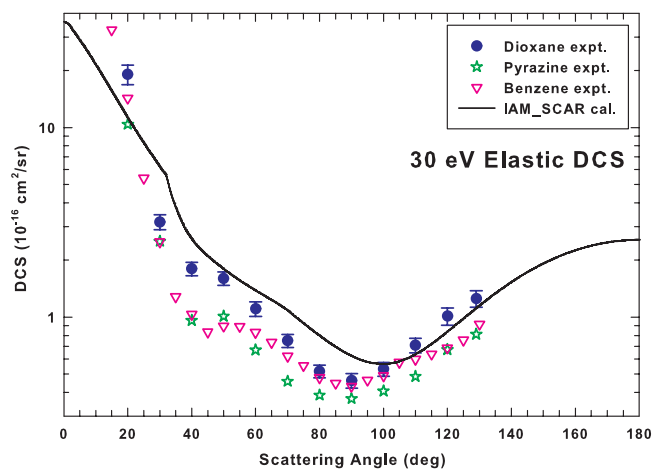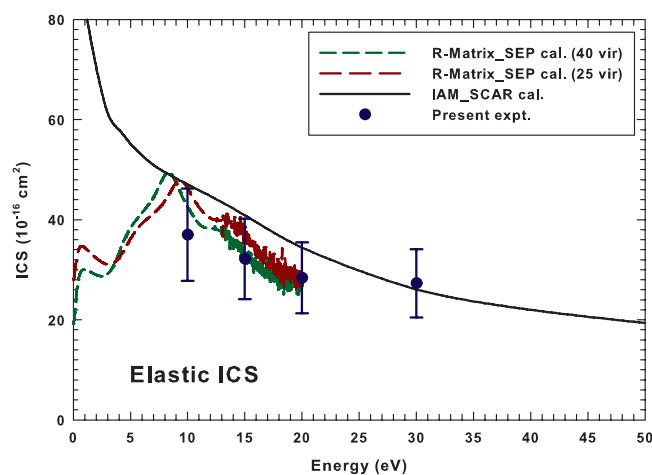

FIG. 5. Absolute DCS for elastic electron scattering from 1,4-dioxane at 20 eV. The present 1,4-dioxane measurements (●) are compared against earlier benzene (▽)[25,26] and pyrazine (☆)[24] results and to our current IAM-SCAR (———) and R-matrix (— — —) 25 virtual orbitals and R-matrix (— · · —) 40 virtual orbital computations.

FIG. 7. Present ICSs for elastic electron scattering from 1,4-dioxane. The measured data are denoted as (●), while our IAM-SCAR (———) and R-matrix (— — —) with 25 virtual orbitals and R-matrix (– – –) with 40 virtual orbital computations are also shown.

Finally, in Fig. 6, we consider the present theoretical and experimental DCS for 30 eV elastic electron scattering from 1,4-dioxane. In this case note, however, we are only able to compare against our IAM-SCAR results, where we now find a fair level of agreement between the measured and calculated DCS. It is certainly the case that this agreement at 30 eV, between our IAM-SCAR theory and measured cross sections, is significantly improved over that we found at the lower energies and consistent with what we have also seen in other systems we have studied.[52,53]

If we now focus on a comparison between the present measured cross sections for 1,4-dioxane and those of benzene[25,26] and pyrazine,[24] in Figs. 3–6, we see that while the data for benzene and pyrazine are almost identical, certainly to within their overall uncertainties (not plotted), the cross sections for 1,4-dioxane, particularly for scattered electron angles greater than about $30° - 40°$, are rather different. As two of the most important physico-chemical properties of these systems, namely, their dipole polarizability and dipole moment, that we might anticipate would drive the scattering dynamics in these three molecules, are very similar in each case, this difference in the DCS, at each energy studied (see Figs. 3–6), initially was a little surprising. Given, however, that the differences in the DCS between 1,4-dioxane, on the one hand, and pyrazine and benzene, on the other, seem to occur at more middle and backward scattering angles, we speculate that this might reflect that the exchange interaction is different in scattering from dioxane compared to pyrazine and benzene. Certainly, 1,4-dioxane has two lone pairs of electrons on each oxygen atom, compared to one lone pair on each nitrogen atom in pyrazine and no lone pairs at all in benzene. Thus, at least intuitively, it is possible to imagine that exchange might be more important in 1,4-dioxane than in either pyrazine or benzene and in Figs. 4–6 it appears, usually, that the magnitude of the respective DCS for scattering angles greater than about 40° is larger in 1,4-dioxane compared to both benzene and pyrazine. Alternatively (or additionally), we note that while benzene and pyrazine are both planar species, 1,4-dioxane is non-planar. This subtle change in geometry, between 1,4-dioxane and the two other molecules, might also contribute to the behaviour we observe in Figs. 4–6. Note further that this proposition could be tested by undertaking similar elastic DCS measurements on cyclohexane.

From the above discussion, we can conclude that there is a quite good shape agreement between the present measured DCS and the R-matrix-SEP calculation for the energies 10, 15, and 20 eV. As a consequence, at each of those energies, we have employed the shape of the relevant R-matrix calculation to extrapolate our measured data to 0° and 180°. Those data are then integrated and multiplied by 2π, resulting in an experimental estimate of the elastic ICS at each of 10, 15, and 20 eV. Those ICS can be found at the foot of Table I and are plotted in Fig. 7, along with the corresponding R-matrix-SEP and IAM-SCAR (see Table II) results. At 30 eV, however, we used the IAM-SCAR theory to perform the backward angle extrapolations with the shape of the 20 eV R-matrix result being employed for the forward angle extrapolation. The resultant 30 eV ICS is also listed in Table I and plotted in Fig. 7. Note that due to the additional uncertainty caused by our ex-

trapolation, we conservatively estimate the errors on our ICS to be ∼25%. It is apparent from Fig. 7 that for energies in the range 10–20 eV the present measured ICS, to within our stated uncertainties, are in very good agreement with our most physical R-matrix-SEP calculation that incorporates 40 virtual orbitals. Where this agreement is poorest (at 10 eV), this is probably due to the resonance (see below) appearing at too high an energy in the calculations. Note that the very narrow peaks present in the R-matrix cross sections above 13 eV are non-physical, but that the general shape of the ICS is correct. Agreement at 30 eV, with the IAM-SCAR calculation, is also found to be excellent.

If we now concentrate on our R-matrix-SEP theory result, again for the case of incorporating 40 virtual orbitals, the following results were obtained. We do not find any conclusive evidence of resonances in the time-delay spectra for the A_g and B_u scattering symmetries. There are, however, at least three features that would merit further investigation with more sophisticated models. The A_u symmetry contains a resonance at 8.36 eV, with a width of 2.83 eV. This resonance is associated mainly with the orbitals $8a_u$ and $10a_u$. In the B_g symmetry we find a shape resonance at 8.30 eV, with a width of 2.25 eV, that appears to be associated with the orbital $7b_g$. Additionally, we find in this symmetry a higher lying feature in the time-delay spectra (apparently associated with the $8b_g$ orbital) which does not have the Lorentzian profile typical for a resonance. The time-delay profile is asymmetric and one part can be fitted accurately by a Gaussian function suggesting that the feature is, in part, non-resonant.[54] It follows therefore that the peak in the R-matrix elastic ICS in Fig. 7 corresponds to two overlapping resonances in A_u and B_u symmetries. We know from our studies in diazine (see e.g., Ref. 23) that our calculations tend to overestimate the position of higher lying shape resonances. We would therefore expect these two resonances to appear at lower energies. Bremner et al.[19] report electron energy loss spectra and claim to see a resonance at around 6.5 eV that enhances the electronic-state excitation. This would further explain why the resonance appears to be too high in energy in the R-matrix calculations: namely, the resonance is likely to have mixed core-excited shape character. A similar resonance appears in pyrazine: it has been shown[23] that these types of resonances can only be accurately represented in our calculations if a diffuse basis set and a carefully chosen set of L^2 functions is used. The electron energy loss spectra of Bremner et al.[19] show the presence of another prominent structure at around 7.5 eV. We cannot ascertain whether this observed structure corresponds in fact to one of the resonances that overlap in our calculations, or if it corresponds to another resonance or to the non-resonant scattering with the Gaussian time-delay profile that our calculations also predict. The shoulder visible at around 5 eV in the R-matrix ICS seems to be non-resonant in origin.

V. CONCLUSIONS

We have reported original measurements, R-matrix calculations and IAM-SCAR calculations, for differential and integral cross sections, for elastic electron scattering from 1,4-dioxane. Agreement between our measured data and the

R-matrix-SEP calculations, for energies ≤20 eV, was typically very good. However, agreement in this lower energy range, with the corresponding IAM-SCAR results was only marginal. Nonetheless at 30 eV, our level of accord between our measured DCS and ICS and the IAM-SCAR computations was now satisfactory. We believe, based on our past experience with other systems,[52,53] that this agreement would improve even further as the energy of the incident projectile is increased. Notwithstanding our belief, it would be very interesting if another group were to specifically investigate the higher energy region.

We also compared the present measured 1,4-dioxane elastic DCS with results, at each energy investigated, from earlier studies on the structurally related compounds benzene[25,26] and pyrazine[24] (see Fig. 1). Note that all three of these organic species have similar dipole moments (∼0 D) and dipole polarizabilities. Whereas, to within the errors on the measurements, the DCS for benzene and pyrazine, at each energy, were virtually identical, the corresponding DCS for 1,4-dioxane, at least for scattering angles greater than about $30 - 40°$, were rather different. We do not have at this time a definitive explanation for this observation, rather we speculated that the additional lone pairs of electrons on each oxygen atom in 1,4-dioxane might lead to an enhanced exchange interaction in the case of electron scattering from 1,4-dioxane. However, it might also be related (in part) to the subtle geometry change between non-planar 1,4-dioxane and planar benzene and pyrazine. Further work is needed to clarify the observed behaviour.

Finally, given the results in Fig. 7, we believe that a reasonably accurate and reliable integral cross section data set, for elastic electron-1,4-dioxane scattering in the energy range 0–1000 eV, might be constructed by "splicing" the low-energy R-matrix results $(0 - 20$ eV) onto the higher energy IAM-SCAR results $(30 - 1000$ eV). Such a data set would be useful for kinetic transport simulations of an electron swarm moving through 1,4-dioxane under the influence of an applied electric and/or magnetic field. It would also be useful for charged-particle track simulations if one were to study the effect of incident radiation moving through a 1,4-dioxane medium.

ACKNOWLEDGMENTS

[1]B. Boudaiffa, P. Cloutier, D. Hunting, M. A. Huels, and L. Sanche, Science **287**, 1658 (2000).

[2]A.-C. Hassan, P.-C. Dugal, and L. Sanche, Radiat. Res. **153**, 23 (2000).

[3]P. L. Levesque, M. Michaud, and L. Sanche, J. Chem. Phys. **122**, 094701 (2005).

[4]A. Muñoz, F. Blanco, G. García, P. A. Thorn, M. J. Brunger, J. P. Sullivan, and S. J. Buckman, Int. J. Mass Spectrom. **277**, 175 (2008).

[5]A. G. Sanz, M. C. Fuss, A. Muñoz, F. Blanco, P. Limão-Vieira, M. J. Brunger, S. J. Buckman, and G. García, Int. J. Radiat. Biol. **88**, 71 (2012).

[6]M. C. Fuss, A. G. Sanz, A. Muñoz, T. P. D. Do, K. Nixon, M. J. Brunger, M.-J. Hubin-Franskin, J. C. Oller, F. Blanco, and G. García, Chem. Phys. Lett. **560**, 22 (2013).

[7]I. Plante and F. A. Cucinotta, New J. Phys. **10**, 125020 (2008).

[8]Z. L. Petrović, S. Marjanović, S. Dujko, A. Banković, G. Malović, S. Buckman, G. Garcia, R. White, and M. Brunger, "On the use of Monte Carlo simulations to model transport of positrons in gases and liquids," Appl. Radiat. Isot. (in press).

[9]R. D. White, W. Tattersall, G. Boyle, R. E. Robson, S. Dujko, Z. L. Petrovic, A. Bankovic, M. J. Brunger, J. P. Sullivan, S. J. Buckman, and G. Garcia, "Low-energy electron and positron transport in gases and soft-condensed systems of biological relevance," Appl. Radiat. Isot. (in press).

[10]C. J. Colyer, V. Vizcaino, J. P. Sullivan, M. J. Brunger, and S. J. Buckman, New J. Phys. **9**, 41 (2007).

[11]M. Fuss, A. Muñoz, J. C. Oller, F. Blanco, D. Almeida, P. Limão-Vieira, T. P. D. Do, M. J. Brunger, and G. García, Phys. Rev. A **80**, 052709 (2009).

[12]T. P. T. Do, M. Leung, M. Fuss, G. Garcia, F. Blanco, K. Ratnavelu, and M. J. Brunger, J. Chem. Phys. **134**, 144302 (2011).

[13]M. C. Fuss, R. Colmenares, A. G. Sanz, A. Muñoz, J. C. Oller, F. Blanco, T. P. D. Do, M. J. Brunger, D. Almeida, P. Limão-Vieira, and G. García, J. Phys.: Conf. Ser. **373**, 012010 (2012).

[14]V. Vizcaino, J. Roberts, J. P. Sullivan, M. J. Brunger, S. J. Buckman, C. Winstead, and V. McKoy, New J. Phys. **10**, 053002 (2008).

[15]P. G. Burke, *R-Matrix Theory of Atomic Collisions: Application to Atomic, Molecular and Optical Processes* (Springer, 2011).

[16]Z. Mašín, J. D. Gorfinkiel, D. B. Jones, S. M. Bellm, and M. J. Brunger, J. Chem. Phys. **136**, 144310 (2012).

[17]H. Kato, K. Anzai, T. Ishihara, M. Hoshino, F. Blanco, G. García, P. Limão-Vieira, M. J. Brunger, S. J. Buckman, and H. Tanaka, J. Phys. B **45**, 095204 (2012).

[18]A. Zecca, E. Trainotti, L. Chiari, M. H. F. Bettega, S. d'A Sanchez, M. T. do N. Varella, M. A. P. Lima, and M. J. Brunger, J. Chem. Phys. **136**, 124305 (2012).

[19]L. J. Bremner, M. G. Curtis, and I. C. Walker, J. Chem. Soc., Faraday Trans. **87**, 1049 (1991).

[20]A. Hinchliffe and H. J. S. Machado, Int. J. Mol. Sci. **1**, 8 (2000).

[21]See http://cccbdb.nist.gov/ for relevant physico-chemical data.

[22]L. Jensen and P. T. van Duijnen, J. Chem. Phys. **123**, 074307 (2005).

[23]Z. Mašín and J. D. Gorfinkiel, J. Chem. Phys. **135**, 144308 (2011).

[24]P. Palihawadana, J. P. Sullivan, S. J. Buckman, and M. J. Brunger, J. Chem. Phys. **137**, 204307 (2012).

[25]H. Cho, R. J. Gulley, K. Sunohara, M. Kitajima, L. J. Uhlmann, H. Tanaka, and S. J. Buckman, J. Phys. B **34**, 1019 (2001).

[26]H. Kato, M. C. Garcia, T. Asahina, M. Hoshino, C. Makochekanwa, H. Tanaka, F. Blanco, and G. García, Phys. Rev. A **79**, 062703 (2009).

[27]J. C. Gibson, L. A. Morgan, R. J. Gulley, M. J. Brunger, C. T. Bundschu, and S. J. Buckman, J. Phys. B **29**, 3197 (1996).

[28]A. Gopalan, J. Bömmels, S. Götte, A. Landwehr, K. Franz, M.-W. Ruf, H. Hotop, and K. Bartschat, Eur. Phys. J. D **22**, 17 (2003).

[29]M. J. Brunger and S. J. Buckman, Phys. Rep. **357**, 215 (2002).

[30]R. K. Nesbet, Phys. Rev. A **20**, 58 (1979).

[31]L. Boesten and H. Tanaka, At. Data Nucl. Data Tables **52**, 25 (1992).

[32]M. J. Brunger, S. J. Buckman, L. J. Allen, I. E. McCarthy, and K. Ratnavelu, J. Phys. B **25**, 1823 (1992).

[33]J. Tennyson, Phys. Rep. **491**, 29 (2010).

[34]J. M. Carr, P. G. Galiatsatos, J. D. Gorfinkiel, A. G. Harvey, M. A. Lysaght, D. Madden, Z. Mašín, M. Plummer, J. Tennyson, and H. N. Varambhia, Eur. Phys. J. D **66**, 58 (2012).

[35]N. Sanna and F. A. Gianturco, Comput. Phys. Commun. **114**, 142 (1998).

[36]T. Kobayashi and S. Nagakura, Bull. Chem. Soc. Jpn. **46**, 1558 (1973).

[37]*NIST Computational Chemistry Comparison and Benchmark Database, NIST Standard Reference Database Number 101*, Release 15b, August 2011, edited by R. D. Johnson III, see http://cccbdb.nist.gov/ (retrieved May 07, 2013).

[38]A. Faure, J. D. Gorfinkiel, L. A. Morgan, and J. Tennyson, Comput. Phys. Commun. **144**, 224 (2002).

[39]M. Tarana and J. Tennyson, J. Phys. B **41**, 205204 (2008).

[40]Z. Mašín and J. D. Gorfinkiel, J. Chem. Phys. **137**, 204312 (2012).

[41]F. Blanco and G. García, Phys. Rev. A **67**, 022701 (2003).

[42]F. Blanco and G. García, Phys. Lett. A **317**, 458 (2003).

[43]F. Blanco and G. García, Phys. Lett. A **330**, 230 (2004).

[44]R. D. Cowan, *The Theory of Atomic Structure and Spectra* (University of California Press, London, 1981).

[45]M. E. Riley and D. G. Truhlar, J. Chem. Phys. **63**, 2182 (1975).

[46]X. Zhang, J. Sun, and Y. Liu, J. Phys. B **25**, 1893 (1992).

[47]G. Staszewska, D. W. Schwenke, D. Thirumalai, and D. G. Truhlar, Phys. Rev. A **28**, 2740 (1983).

[48]F. Blanco and G. García, Phys. Lett. A **295**, 178 (2002).

[49]O. Zatsarinny, K. Bartschat, G. Garcia, F. Blanco, L. R. Hargreaves, D. B. Jones, R. Murrie, J. R. Brunton, M. J. Brunger, M. Hoshino, and S. J. Buckman, Phys. Rev. A **83**, 042702 (2011).

[50]J. B. Maljković, A. R. Milosavljević, F. Blanco, D. Šević, G. García, and B. P. Marinković, Phys. Rev. A **79**, 052706 (2009).

[51]F. Blanco and G. García, J. Phys. B **42**, 145203 (2009).

[52]P. Palihawadana, J. Sullivan, M. Brunger, C. Winstead, V. McKoy, G. Garcia, F. Blanco, and S. Buckman, Phys. Rev. A **84**, 062702 (2011).

[53]H. Kato, A. Suga, M. Hoshino, F. Blanco, G. García, P. Limão-Vieira, M. J. Brunger, and H. Tanaka, J. Chem. Phys. **136**, 134313 (2012).

[54]R. H. Dalitz and R. G. Moorhouse, Proc. R. Soc. A **318**, 279 (1970).